Mousa *et. al.,* Babcock Univ. Med. J.2025 8(2):339-349
https://doi.org/10.38029/babcockuniv.med.j..v8i2.1073
eISSN: 2756-4657

RESEARCH ARTICLE OPEN ACCESS

Synthesis, Biological Evaluation, and Molecular Docking of Novel Pyrazole-Nitrone Derivatives as EGFR-targeted Anticancer Agents

Mousa NAJ[1ID], Salman HH[1ID], Alsaad HN[1ID]

[1]*Department of Pharmaceutical Chemistry, College of Pharmacy, University of Basrah, Iraq*

Submitted: 5th March 2025
Accepted: 2nd August 2025
Published: 31st December 2025
ID: Orcid ID

Abstract
Objective: This study aimed to design, synthesise, and characterise some novel pyrazole-nitrone derivatives and evaluate their potential as anticancer agents targeting EGFR-expressing lung cancer cells. Biological evaluation included cytotoxicity assessment against A549 (lung cancer) and HdFn (normal fibroblast) cell lines, alongside in-silico docking and ADME profiling to predict drug-likeness and pharmacokinetic behaviour. We hypothesised that the presence of electron-donating groups (EDGs) at the para position of the aryl ring would enhance the cytotoxicity and selectivity of the nitrone derivatives by improving their interaction with EGFR and reducing off-target toxicity.
Methods: The synthesis started with the Vilsmeier-Haack reaction to prepare 4-formyl-3-(3-nitrophenyl)-1-phenyl-1H-pyrazole. N-substituted phenylhydroxylamines were obtained by reducing nitrobenzene derp tolylivatives, followed by condensation with the aldehyde to afford nitrones. The synthesised compounds were evaluated for anticancer activity against A549 lung cancer cells and HdFn normal dermal fibroblast cells using the MTT assay. Additionally, molecular docking studies were performed to investigate interactions with the EGFR tyrosine kinase.
Results: The IC_{50} values indicated that compound 7a exhibited the most potent activity, with an IC_{50} of 85.62 µg/mL against A549 cells and a high selectivity index (SI) of 5.5. Pre-ADME in silico analyses showed favourable oral bioavailability and no predicted CNS side effects for all tested compounds.
Conclusion: Spectroscopic data from FT-IR, ^{1}H-NMR, and ^{13}C-NMR confirmed successful target compound syntheses. Biological evaluation revealed that compound 7a demonstrated promising anticancer activity with a favourable selectivity index (SI = 5.5) toward cancer cells over normal cells, indicating its potential as a promising EGFR-targeted therapeutic agent.

Keywords: Nitrone compounds, Pyrazole, A549 cell, Docking study, *pre*-ADME study

Plain English Summary

These compounds were designed in the lab and carefully analysed to confirm their structure using different techniques. Tested the effects of these compounds on human lung cancer cells (A549) and compared them to their effects on normal cells. One of the compounds, designated as 7a, exhibited potent anticancer activity and demonstrated a particular affinity for targeting cancer cells without harming healthy ones. In addition, computer simulations (called molecular docking) showed that these compounds could effectively bind to a key protein (EGFR) involved in cancer growth. The study also utilised specialised tools to predict how the compounds behave within the body, including their absorption rates, safety profiles, and potential for side effects. Overall, this research highlights compound 7a as a promising starting point for developing new cancer treatments with fewer side effects.

Correspondence:
Mousa, Noor AA
Department of Pharmaceutical Chemistry,
College of Pharmacy,
University of Basrah,
Iraq
pgs.nooralhuda.jaleel@uobasra.edu.iq

Introduction

Non-small cell lung cancer (NSCLC) remains the leading cause of cancer-related mortality worldwide, accounting for approximately 85 % of lung cancer cases and featuring a 5-year survival rate below 15 % (1). Among NSCLC subtypes, overexpression or activating mutations in the epidermal growth factor receptor (EGFR) drive malignant behaviour through continuous activation of downstream signalling pathways such as RAS/MAPK and PI3K/AKT, promoting proliferation, inhibiting apoptosis, and facilitating metastasis (2). Specifically, the A549 human lung adenocarcinoma cell line expresses elevated levels of EGFR and HER2, making it a widely accepted in vitro model for assessing EGFR-targeted therapeutics (3). Given the critical role of EGFR in NSCLC, tyrosine kinase inhibitors such as gefitinib, erlotinib, and osimertinib have become foundational in targeted therapy. However, their clinical efficacy is often limited by acquired resistance mechanisms, notably the T790M mutation, which elevates ATP affinity and diminishes inhibitor binding (4). This underscores the pressing need for new molecular scaffolds capable of effective EGFR inhibition with improved selectivity and resistance profiles. Pyrazole derivatives have emerged in recent years as versatile scaffolds in anticancer drug discovery, demonstrating potent activities and favourable selectivity indices in both in vitro and in vivo models (5). Significantly, hybrid molecules combining pyrazole cores with nitrone moieties may offer dual advantages: the kinase-inhibitory potential of pyrazole and the radical-trapping, redox-modulating features of nitrones. Such hybrids have started to attract attention as promising anticancer agents (6). Therefore, designing pyrazole-nitrone hybrids as EGFR-targeted anticancer agents represents a rational approach: the pyrazole structure supports binding in the ATP-pocket of the EGFR kinase domain, while the nitrone fragment may confer redox-mediated selectivity toward malignant cells. This combination is expected to enhance potency against EGFR-overexpressing NSCLC cells such as A549, while minimising toxicity to normal fibroblasts, justifying the therapeutic hypothesis of this study (7).

Materials and Methods

Necessary materials were sourced directly from existing supplies, ensuring a convenient and efficient process without the delays of additional purification. Melting points were accurately determined using a state-of-the-art digital Electrothermal IA 9100 Series apparatus, guaranteeing reliable results. FT-IR spectra were recorded with an FT-IR Shemidz–8100S plus spectrometer, which operates within a range of 4000 to 400 cm^{-1}, utilising KBr disc. NMR spectra were obtained using an Inova NMR spectrometer (400 MHz, ^{1}H-NMR) and (100 MHz for ^{13}C-NMR) spectra in DMSO-d_6 as solvent. The chemical shifts are stated in (ppm).

Synthesis of the hydrazone derivative of 3-nitroacetophenone (8)

In a round-bottom flask (150 mL), Phenylhydrazine 1 (0.02 mol) and four to five drops of G. AcOH were added to a solution of 1-(3-nitrophenyl) ethenone 2 (0.02 mol) in 25 mL of absolute ethanol. The reaction was stirred at 75–85°C for up to 2 hrs. Afterwards, it was allowed to stand overnight. The product **3** was filtered and purified with ethanol, yield (4.30 g, 84.8%), m. p 130-132^{o}C. The purity was assessed using thin-layer chromatography (TLC) with a hexane and ethyl acetate mixture (7:3) as the eluent.

Synthesis of 4-formyl-3-(3-nitrophenyl)-1-phenyl-1H-pyrazole (9)

In a well-prepared 150 mL round-bottomed flask, add equimolar phosphoryl chloride to cold dimethylformamide (DMF) while stirring slowly for 30 minutes. This careful addition ensured optimal reaction conditions. The mixture should be maintained at 0°C for 40 minutes to promote stability. Compound **3** (0.02 mol) was then added. The reaction proceeded by heating to 90°C, with continuous stirring for four hours, allowing for thorough interaction. crushed ice was added to the mixture after it cooled and was slowly neutralised with NaOH. The resulting desired compound was effectively filtered, dried, and recrystallised using a precise chloroform: methanol ratio of 1:1. The impressive yield of 4.8 g (82.7%) and a melting point of 160-165°C underscore the efficiency and success of this synthesis.

Synthesis of N-substituted phenylhydroxylamine (6a-6d) (10)

In a conical flask (150 mL), ammonium chloride (0.05 mol), 100 mL of water and substituted nitrobenzene (5a-5d) (0.04 mol) were mixed with stirring. Gradually add (0.15) mol of zinc dust to the stirred mixture. As the reduction proceeds, the temperature rises to 60–65°C. Stirring was continued for 15 min. At the end of this time, the hot mixture was carefully filtered. Next, a saturated sodium chloride (NaCl) solution was applied to the filtrate that was produced. The saturated filtrate is cooled with an ice-salt mixture to precipitate hydroxylamine. The desired N-substituted phenylhydroxylamine is then filtered, dried, and recrystallised using a toluene and petroleum ether mixture.

Synthesis of nitrones derivatives (7a-7d) (11)
An equimolar mixture of aldehyde 4 and N-substituted-phenylhydroxylamines (6a-6d) was carefully dissolved in 30 ml of dioxane and stirred for an extended period overnight. This process allowed for the efficient formation of the nitrone, which was then filtered out and successfully recrystallised using a blend of dioxane and methanol, ensuring purity and optimal yield of the desired compound.

Docking study
Molecular docking studies were conducted to assess the binding affinity of the synthesised compounds (7a–7d) to the active site of EGFR tyrosine kinase. The protein structure was retrieved from the Protein Data Bank (PDB ID: 4HJO), and preparation involved removal of water molecules and energy minimisation (https://www.rcsb.org). All ligands were optimised using the MMFF94 (Merck Molecular Force Field) to ensure realistic geometry. Docking was performed using MOE 19.0901 software, employing the London dG scoring function to estimate binding free energy (ΔG) values. A total often poses were generated for each compound, and the best-ranked pose was selected based on the lowest binding energy and proper orientation within the binding pocket. Validation of the docking protocol was performed by redocking the co-crystallised ligand, and an RMSD cutoff of <2.0 Å was used to ensure reliable alignment.

Physicochemical properties of Pyrazole-Nitrone compounds
The pharmacokinetic and drug-likeness properties of the synthesised compounds (7a–7d) were predicted using the SwissADME online platform (https://www.swissadme.ch/). The assessment included key parameters aligned with Lipinski's Rule of Five, which evaluates drug-likeness based on the following criteria:
Molecular weight (MW < 500 g/mol).
Octanol-water partition coefficient (Log P < 5).
Number of hydrogen bond donors (HBD ≤ 5).
Number of hydrogen bond acceptors (HBA ≤ 10).
Additional descriptors such as the Topological Polar Surface Area (TPSA), number of rotatable bonds (NRB), gastrointestinal (GI) absorption, blood-brain barrier (BBB) permeability, and P-glycoprotein (P-gp) substrate potential were also analysed to estimate oral bioavailability, CNS safety, and efflux susceptibility (12, 13, 14). All data were recorded and interpreted based on the generated SwissADME profiles.

Cell viability assay
In the current study, the MTT screening was employed for evaluating the cellular toxicity of synthetic compounds (7a-7d) using A549 cells, and human HdFn as normal cells. Cells were maintained as described in (15). The absorbing capacity of formed formazan was determined at 570 nm utilising an ELISA microplate reader (Bio-Rad, USA).

Statistical analysis
Using Duncan's test to determine the significance of group variance, one-way analysis of variance (ANOVA) was used. For this test, the statistical designation was established at $p \leq 0.05$. The findings are effectively presented as mean ± standard deviation; all statistical calculations were performed using GraphPad Prism 6 (GraphPad Software Inc., La Jolla, CA). This rigorous approach ensures the reliability and validity of the results.

Results
Chemistry
The titled compound 4 was obtained (Scheme 1) from the 3-nitroacetophenone and phenylhydrazine under reflux conditions and transformed via Vilsmeier-Haack reagent using $POCl_3$ and DMF to get 4-formyl-3-(3-nitrophenyl)-1-phenyl-1*H*-pyrazole 4. Four different *N*-substituted phenylhydroxylamines 6a-6d were obtained from the reduction reaction of nitrobenzene derivatives with zinc dust (Scheme 1). The reaction of 4 with *N*-substituted phenylhydroxylamines under stirring overnight, 6a-6d, affords the title nitrones 7a-7d (Scheme 1). Table 1 summarises the properties of the intermediate compound.

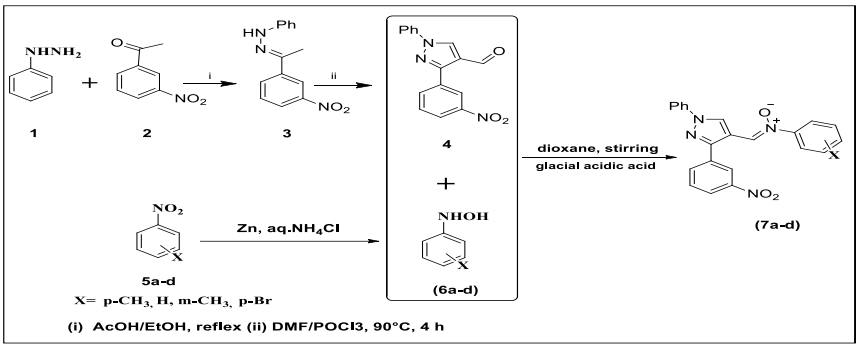

Scheme 1: Chemical synthesis of target compounds (7a-7d)

Table 1: Physical properties of all intermediate compounds

Compound	Chemical formula	Molecular weight	Melting point (°C)	Colour	Yield (%)
3	$C_{14}H_{13}N_3O_2$	255.28	130-132	Orange	84.3
4	$C_{16}H_{11}N_3O_3$	293.28	160-165	White	82.7
6a	C_7H_9NO	123.16	95-96	Yellow	77.2
6b	C_6H_7NO	109.13	65-67	White	93.3
6c	C_7H_9NO	123.16	78-80	White	85.7
6d	C_6H_6BrNO	188.02	98-100	Yellow	90.05

1-(3-(3-Nitrophenyl)-1-phenyl-1H-pyrazol-4-yl)-N-(p-tolyl)methanamineoxide (7a)
Yield (3.3 g, 82.9 %) as a pale yellowish powder, m.p. 170-172. FT-IR (KBr disc/ cm^{-1}): 3163(-CH, aromatic), 2860, 2918 (C-H, aliphatic), 1595 (-C=N), 1587,1446 (C=C), 1342 (N-O), 688 (-CH, aromatic) out of plane bending. ^{1}H NMR: δ= 2.36 (s) (3H, CH_3), 9.84(s) (1H), 8.53(s) (1H), 8.35(s) (1H) ,8.33(dt) (1H), 8.31(dt) (1H). ^{13}C NMR: 21.37 -$C_{(Methyl)}$, 135.38 -$C=N_{(Pyrazole)}$, 139.9 -$C=C_{(Pyrazole)}$, 145.7 $C_{(-NO2, Aromatic)}$, 148.6 $C_{(-NO2, Aromatic)}$, 150.6 $C_{(Imine-oxide)}$.

1-(3-(3-nitrophenyl)-1-phenyl-1H-pyrazol-4-yl)-N-phenylmethanimineoxide (7b)
Yield (3.2 g, 83.3 %) as a pale yellowish powder, m.p. 174-176. FT-IR (KBr disc/ cm^{-1}), 3078, 3157 (-CH, aromatic), 1595 (-C=N), 1568, 1462 (C=C), 1354 (N-O), 692(-CH, aromatic) out of plane bending. ^{1}H NMR: δ= 9.89(s) (1H), 8.5(s) (1H), 8.40(s) (1H), 8.35(dt) (1H), 8.33(dt) (1H). ^{13}C NMR: 135.4 -$C=N_{(Pyrazole)}$, 139.2 -$C=C_{(Pyrazole)}$, 148.0 $C_{(-NO2-Aromatic)}$, 148.6 $C_{(-NO2-Aromatic}$, 150.7 $C_{(Imine-oxide)}$.

1-(3-(3-nitrophenyl)-1-phenyl-1H-pyrazol-4-yl)-N-(m-tolyl)methanimineoxide (7c)
Yield (3.5 g, 87.9 %) as a yellowish powder, m.p 211-213 °C. FT-IR (KBr disc/ cm^{-1}): 3169 (-CH, aromatic), 1598 (-C=N), 1579, 1413 (C=C), 1535 (N-O), 688 (-CH, aromatic) out of plane bending. ^{1}H-NMR: δ= 2.38(s) (3H, CH_3), 9.84(s) (1H), 8.52(s) (1H), 8.33(s) (1H), 8.31(dt) (1H), 8.27(dt) (1H). ^{13}C-NMR: 21.3 $C_{(Methyl)}$, 135.3 $C=N_{(Pyrazole)}$, 139.2 $C=C_{(Pyrazole)}$, 148.0 $C_{(-NO2-Aromatic}$, 148.6 $C_{(-NO2-Aromatic}$, 150.6 $C_{(Imine)}$.

N-(4-bromophenyl)-1-(3-(3-nitrophenyl)-1-phenyl-1*H*-pyrazol-4-yl) methanimineoxide (7d)
Yield (4.1 g, 88.7 %) as a yellowish powder, m.p 215-217 °C. FT-IR (KBr disc/ cm^{-1}): 3194, 3062 (-CH, aromatic), 1600 (-C=N), 1579, 1429 (C=C). 1504 (N-O), 908 (-CH, aromatic) out of plane bending. ^{1}H NMR: δ= 9.87(s) (1H), 8.54(s) (1H), 8.42(s) (1H), 8.34(dt) (1H), 8.28(dt) (1H). ^{13}C NMR: 135.53 $C=N_{(Pyrazole)}$, 139.2 $C=C_{(Pyrazole)}$.

The 1H NMR and 13C NMR spectra of compound 7a are illustrated in Figure 1. This figure depicts the chemical scaffold common to the pyrazole-nitrone derivatives (7a–7d). The structural core includes a pyrazole ring, with substitutions influencing their physicochemical and biological properties. This serves as the foundational template for SAR (structure–activity relationship) considerations.

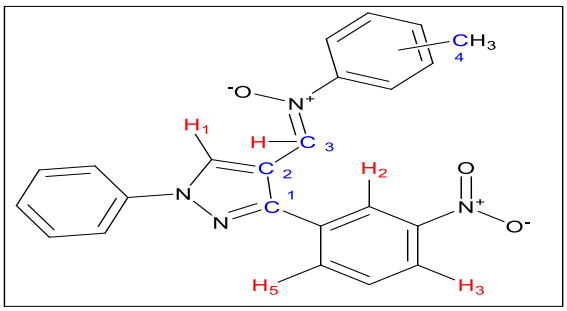

Figure 1: General structure of synthesised compounds 7a

Molecular docking

Figure 2 presents both 2D and 3D docking orientations of the synthesised compounds and the reference drug erlotinib within the EGFR tyrosine kinase active site. The docking analysis shows that the test compounds interact favourably with key amino acid residues, forming hydrogen bonds, hydrophobic contacts, and π–π stacking interactions. Notably, compound 7a exhibits stable interactions similar to erlotinib, indicating its potential as a lead candidate.

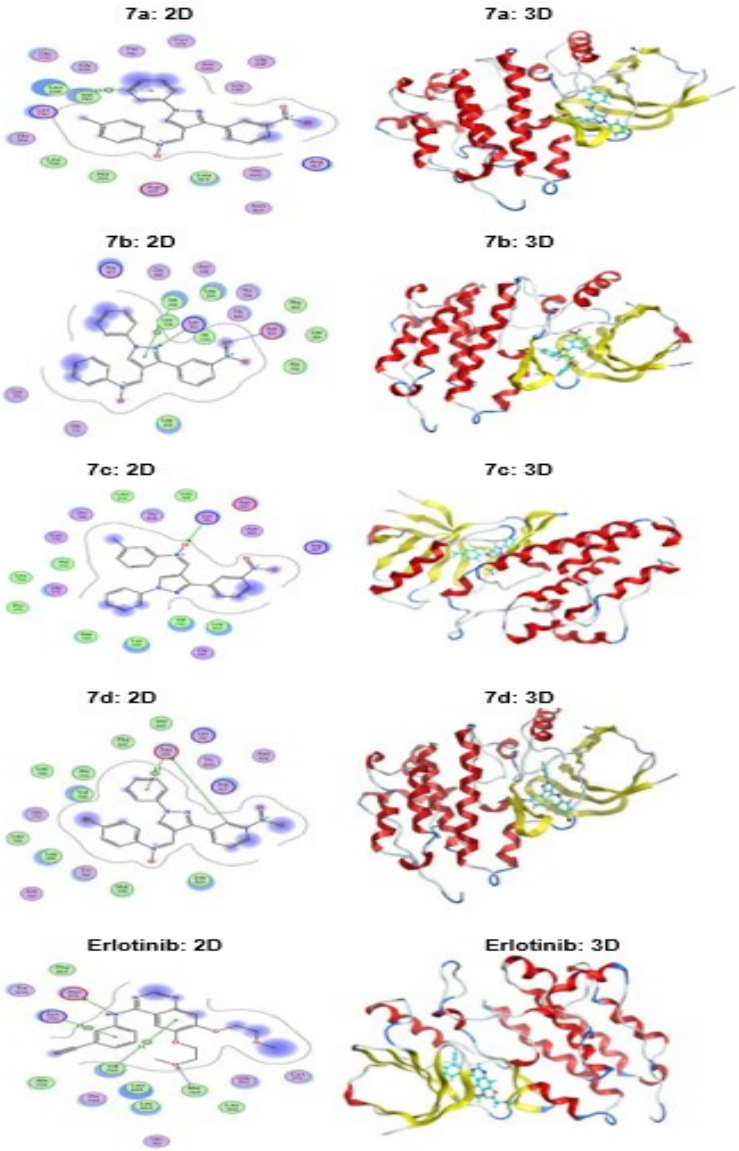

Figure 2: 2D and 3D orientation of Erlotinib and synthesised compounds (7a-7d) docked in EGFR tyrosine kinase

Table 2 displays the molecular docking results of compounds 7a–7d against EGFR (PDB ID: 4HJO). All compounds demonstrated good binding affinity, with compound 7c showing the highest docking score (-7.52 kcal/mol), though erlotinib remained the strongest binder (-8.30 kcal/mol). RMSD values below 2.0 Å indicate acceptable docking accuracy for all ligands.

Table 2: Docking Scores and RMSD Values for Compounds 7a–7d and Erlotinib

Compound	Docking Score ΔG kcal/mol	RMSD (A˚)
7a	-7.01	1.03
7b	-7.51	1.74
7c	-7.52	0.89
7d	-6.48	0.87
Erlotinib	-8.30	1.28

RMSD: Root Mean Square Deviation

Physicochemical Properties of Synthesised Compounds 7a–7d and Erlotinib

Table 3 outlines molecular weights, hydrogen bond donors and acceptors, lipophilicity (Log P), and total polar surface area (TPSA). All synthesised compounds complied with Lipinski's rule of five, suggesting good oral bioavailability. Water solubility was uniformly poor (P), and compound 7d, with the highest Log P (3.84), may pose formulation challenges. Erlotinib, used as the reference, had similar parameters but more rotatable bonds and hydrogen bond acceptors.

Table 3: Physicochemical Properties of Synthesised Compounds 7a–7d and Erlotinib

Comp.	Chem.	M.W	NRB	NHA	NHD	TPSAA^{o2}	Water	Log p	Lipinski
7a	$C_{23}H_{18}N_4O_3$	398.42	5	4	0	92.39	P	3.37	Yes:0 violation
7b	$C_{22}H_{16}N_4O_3$	384.39	5	4	0	92.39	P	3.21	Yes:0 violation
7c	$C_{23}H_{18}N_4O_3$	398.42	5	4	0	92.39	P	3.38	Yes:0 violation
7d	$C_{22}H_{15}BrN_4O_3$	463.29	5	4	0	92.39	P	3.84	Yes:0 violation
Erlotinib	$C_{22}H_{23}N_3O_4$	393.44	10	6	1	74.73	P	3.23	Yes:0 violation

NRB = No. of rotatable bonds, NHA = No. H-bonds acceptors, NHD = No. H-bonds donors, TPSA = total polar surface area, Log p = Lipophilicity (Log $P_{o/w}$), P = Poorly water soluble.

Pharmacokinetic Predictions of Synthesised Compounds (7a–7d)

Table 4 summarises the key ADME (absorption, distribution, metabolism, and excretion) properties predicted using SwissADME. All test compounds exhibited high gastrointestinal absorption, but none were predicted to cross the blood–brain barrier or serve as P-glycoprotein substrates. Each compound was also predicted to inhibit at least one cytochrome P450 enzyme, indicating possible drug–drug interaction potential. These results support the drug-likeness of the synthesised compounds.

Table 4: Pharmacokinetic Predictions of Synthesised Compounds (7a–7d)

Name	GI abs.	BBB permeant	P-gp. Subs.	Enzyme inhibitors
7a	High	-	-	+
7b	High	-	-	+
7c	High	-	-	+
7d	High	-	-	+
Erlotinib	High	+	-	+

GI abs. = gastric intestine absorption, BBB=blood brain barrier, P-gp Subs.= P-glycoprotein substrate. (-) = No, (+) = Yes.

In vitro study anticancer activity of compounds 7a-d

Figure 3 shows the dose-response cytotoxicity curves of the synthesised compounds against the A549 lung cancer cell line and HdFn normal fibroblasts. Among all, compound 7a demonstrated the most potent activity against A549 cells while maintaining low toxicity to normal cells, confirming its favourable selectivity profile.

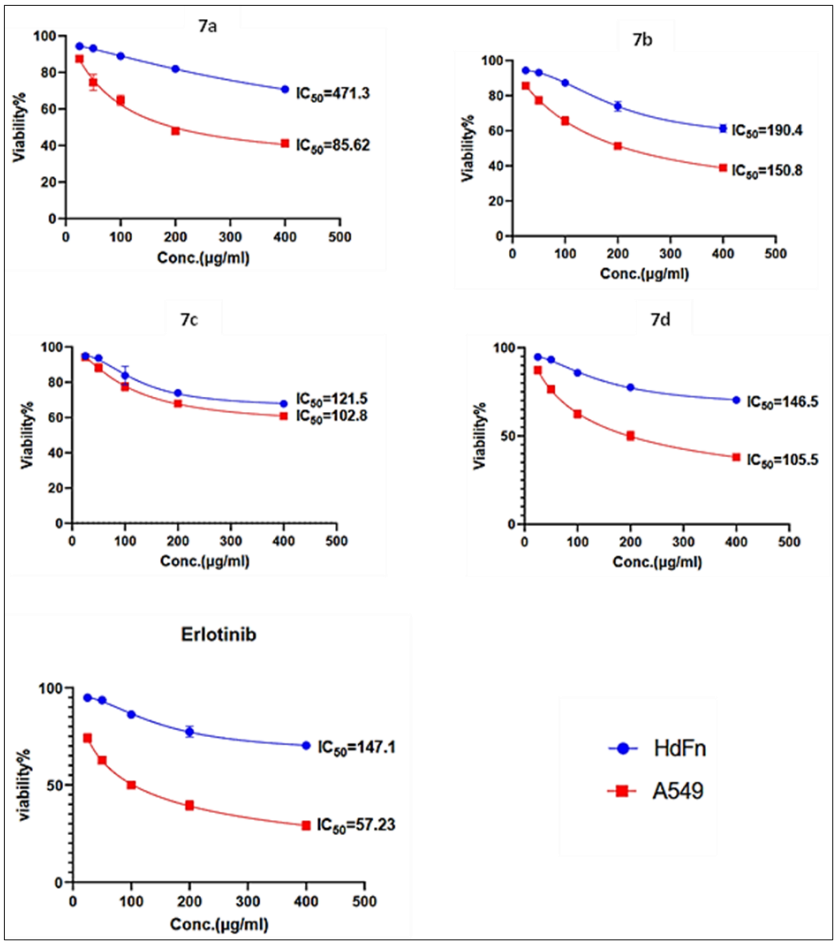

Figure 3: Cytotoxic Effects of Compounds 7a–7d Against A549 Lung Cancer Cells and Normal Lung Fibroblasts (HdFn)

Table 5 summarises the in vitro cytotoxic effects of the test compounds. Compound 7a exhibited the lowest IC_{50} against A549 (85.62 µg/mL) and the highest IC_{50} against normal cells (471.3 µg/mL), resulting in the highest selectivity index (SI = 5.5). This indicates a better therapeutic window compared to erlotinib (SI = 2.57), highlighting 7a as a promising anticancer candidate.

Table 5: Cytotoxicity Data: IC_{50} Values and Selectivity Indices for Compounds 7a–7d and Erlotinib

Compound	HdFn IC_{50} (µg\mL)	A549 IC_{50} (µg\mL)	SI
7a	471.3	85.62	5.50
7b	190.4	150.8	1.26
7c	121.5	102.8	1.15
7d	146.5	105.5	1.38
Erlotinib	147.1	57.23	2.57

Full spectral data (FT IR, ^{1}H NMR, ^{13}C NMR) and docking poses for compounds 7a–7d are provided in the supplementary data file.

Discussion

All synthesised pyrazole-nitrone compounds were identified with spectral data that confirmed the proposed structures. FT- IR spectra of pure compounds 7a-d showed a new typical band at 1595-1600 cm^{-1} assigned to the vibrations of C=C and C=N groups. The key diagnostic feature supporting nitrone formation was the disappearance of the characteristic aldehyde C=O absorption band at ~1680 cm^{-1} in the FT-IR spectrum, indicating complete condensation with hydroxylamines. Concurrently, a new band appeared in the region 1595–1600 cm^{-1}, assigned to the C=N bond of the nitrone moiety, along with distinct N–O stretches (1342–1535 cm^{-1}), confirming successful cycloaddition (16). The bands at 688-958 cm^{-1} and 3055-3194 cm^{-1} are related to the bending and stretching

vibrations of the aromatic C-H, respectively (17,18). The bands appeared at (1535-1500 cm^{-1}) and (1342-1386 cm^{-1}) correlated with symmetrical and asymmetrical vibrations, respectively, to the —NO_2 group (19, 20). The IR spectra of 7a-d compounds showed a characteristic vibration in the region 1413–1587 cm^{-1} related to the aromatic C=C group (21).

The ^{1}H-NMR spectra of 7a-7d compounds in DMSO-d_6 revealed characteristic singlet signals at 2.50-2.51 ppm attributed to –CH=NO proton, and singlet signals at 9.84-9.89 ppm and 8.33-8.41ppm attributed to proton H-2 and H-3, respectively (22). Besides, a doublet signal was detected at 8.31-8.35 (ppm) corresponding to the proton H-5. The ^{1}H-NMR spectra of pyrazole derivatives revealed a significant singlet signal at 8.41-8.55 ppm attributed to the proton H-1 (23).

Additionally, the ^{13}C-NMR spectra showed characteristic signals at 135.3-135.5 ppm, 139.2-1139.9 ppm and 150.6- 150.7 ppm for atoms C-1, C-2 and C-3, respectively (24). Moreover, the ^{13}C-NMR spectra showed signals at regions 145.75-148.0 ppm and 148.6 ppm for C-4 and C-5 atoms, respectively (25). Compounds 7a and 7c showed signals at 21.3 Ppm and 21.0 ppm corresponding to the methyl group (26).

The crystal ligand Erlotinib exhibits a remarkably strong binding affinity, with an energy of binding of -8.303 kcal/mol when interacting with EGFR tyrosine kinase, highlighting its potential as an effective therapeutic agent. Erlotinib formed two H-π interactions with Lys 721 and Val 702, and additionally, it formed two hydrogen bonds between the O-methoxy atom and NH with Met 769 and Asp 831, respectively (27). Compound 7a exhibited a binding energy of -7.014 kcal/mol, which was slightly lower than that of erlotinib (-8.30 kcal/mol), yet still indicative of strong binding affinity; it forms one hydrogen-π interaction bond with Leu 694. In contrast, compound 7b shows a binding energy of -7.516 kcal/mol. It establishes a hydrogen-π interaction between the pyrazole ring and Val 702. In addition to forming two H-bonds between the N-pyrazole and Lys 721, and between the oxygen of the nitro group and Asp 831. Compound 7c has a binding energy of -7.522 kcal/mol. The Nitro group also generates an H-bond with Lys 721. Conversely, Compound 7d shows the energy of binding -6.481 kcal/mol, with its binding mode indicating two π interactions between its aromatic rings and Asp 831(28). These results support the potential of these derivatives as effective EGFR-targeted agents.

The physicochemical and pharmacokinetic properties demonstrate that all the designed compounds meet the essential criteria for oral absorption. Since their molecular weights are all below 500 g/mol, it is evident that NRB 5 demonstrates a favourable balance between molecular flexibility, oral bioavailability, and permeability. NHA had a value of 4, indicating a limited capacity for hydrogen bonding along with a highly lipophilic character, as suggested by an NHD zero. These factors could influence the solubility and binding interactions with biological targets. We noticed in Table 3 that all compounds have a total surface area (TPSA) of 92.39. Despite the promising biological activity, Table 2 indicates that all compounds exhibited poor aqueous solubility, which could limit their bioavailability in physiological environments. To address this limitation, future studies should explore formulation strategies such as nanoemulsions, lipid-based delivery systems, or polymeric micelles. These platforms have shown success in improving solubility, cellular uptake, and tumour accumulation of poorly soluble drugs, and could significantly enhance the therapeutic potential of pyrazole-nitrone derivatives (29). Despite the good gastrointestinal (GI) absorption of the compounds, pharmacokinetic property Analyses showed that no compound could penetrate the blood-brain barrier. This characteristic suggests that they are less likely to produce negative central nervous system (CNS) effects after use. Additionally, none of the study compounds act as P-glycoprotein (P-gp) substrates. This feature could be advantageous for drugs targeting specific tissues or organs, such as anticancer drugs, where P-gp efflux presents a limiting factor. However, it also means that careful monitoring may be required to prevent the accumulation of these compounds in certain tissues (30). Most of the compounds analysed in this study were enzyme inhibitors. To reduce the risk of drug interactions, it is important to allow a gap between the administration of these substances and other medications.

MTT assay was used to evaluate the in vitro anticancer activity against the human lung cancer cell line A549 and HdFn as a normal cell (31). From the dose-response curve, the maximum inhibitory concentration (IC_{50}) was determined by measuring the percentage of cells remaining at different concentrations of the compounds, as noted in Figure 3. Compounds that exhibited anticancer specificity had a selectivity index (SI) higher than 1.0. are considered highly selective. The prepared compounds showed cytotoxicity within the range of 85.62-150.8 µg/mL, as displayed in Table 5. Among the synthesised derivatives, compound **7a** demonstrated the most potent and selective anticancer activity with an IC_{50} of 85.62 µg/mL

and a selectivity index (SI) of 5.5, compared to erlotinib, which had an SI of 2.57. This enhanced selectivity of 7a may be attributed to the presence of a para-methyl (*p-tolyl*) substituent, an electron-donating group (EDG) that likely increases electron density across the nitrone system. This may enhance the compound's ability to selectively interact with the electron-deficient ATP-binding pocket of EGFR in cancer cells, while exhibiting lower reactivity toward normal cells. Moreover, the methyl group may contribute to improved π–π interactions with hydrophobic residues such as Leu694 or Val702, supporting stronger binding affinity in docking simulations (28).

Conclusion

In conclusion, a novel series of pyrazole-nitrone derivatives was successfully synthesised and structurally characterised. Compound 7a emerged as the most promising candidate, exhibiting significant anticancer activity against A549 lung cancer cells with a high selectivity index (SI = 5.5), outperforming the reference drug erlotinib. Molecular docking and ADME studies further supported its potential as an EGFR-targeted agent with favourable pharmacokinetic and safety profiles.

To strengthen the translational relevance of these findings, future studies should focus on evaluating the in vivo efficacy of compound 7a using xenograft tumour models, particularly to confirm its selectivity and systemic safety. Additionally, structural optimisation strategies such as PEGylation or prodrug design may be explored to overcome the solubility limitations identified in silico, without compromising the compound's anticancer activity or target affinity.

List of Abbreviations

A549: Adenocarcinomic human alveolar basal epithelial cell
HdFn: Human dermal fibroblast normal
IC_{50}: 50% maximal inhibitory concentration
MTT: 3-(4,5-dimethylthiazol-2-yl)-2,5-diphenyltetrazolium bromide
EGFR: Epidermal growth factor receptor
ADME: Absorption, Distribution, Metabolism, and Excretion

Declarations

Ethical statement

The cytotoxicity assays in this study were conducted using commercially available human cell lines (A549 and HdFn). Therefore, institutional ethical approval was not required. No human or animal subjects were involved.

Consent for publication

All the authors gave consent for the publication of the work under the Creative Commons Attribution-Non-Commercial 4.0 license

Supplementary Information

Full spectral data (FT-IR, ^{1}H-NMR, ^{13}C-NMR) and docking poses for compounds 7a–7d are provided in the supplementary file.

Competing interests

The authors declare no conflict of interest.

Funding

Nil.

Authors' contributions

This research was conducted as part of the master's thesis of MNAJ, under the supervision of SHH and AHN. MNAJ carried out the synthesis, experimental work, data analysis, and initial drafting of the manuscript. SHH and AHN provided conceptual guidance, supervised all stages of the research, contributed to data interpretation, and critically revised the manuscript. All authors reviewed and approved the final version of the manuscript.

Acknowledgement

The authors thank the College of Pharmacy, University of Basrah, Iraq, for providing the facilities and support to conduct this research.

References

1. Özdemir A, Ciftci H, Sever B, Tateishi H, Otsuka M, Fujita M. A New Series of Indeno[1,2-c]pyrazoles as EGFR TK Inhibitors for NSCLC Therapy. Vol. 27, Molecules. 2022. https://doi.org/10.3390/molecules27020485
2. Zhou P, Hu J, Wang X, Wang J, Zhang Y, Wang C. Epidermal growth factor receptor expression affects proliferation and apoptosis in non-small cell lung cancer cells via the extracellular signal-regulated kinase/microRNA 200a signaling pathway. Oncol Lett. 2018;15(4):5201–7. https://doi.org/10.3892/ol.2018.7961
3. Diaz R, Nguewa PA, Parrondo R, Perez-Stable C, Manrique I, Redrado M, et al. Antitumor and antiangiogenic effect of the dual EGFR and HER-2 tyrosine kinase inhibitor lapatinib in a lung cancer model. BMC Cancer. 2010;10. https://doi.org/10.1186/1471-2407-10-188
4. Yun CH, Mengwasser KE, Toms A V., Woo MS, Greulich H, Wong KK, et al. The T790M mutation in EGFR kinase causes drug resistance by increasing the affinity for ATP. Proc Natl Acad Sci U S A. 2008;105(6):2070–5. https://doi.org/10.1073/pnas.0709662105

5. Mahmoud SE, Fadda AA, Abdel-Latif E, Elmorsy MR. Discovery and molecular characterization of a potent thiazolyl-pyrazole hybrid targeting EGFR for breast cancer therapy. Sci Rep. 2025;15(1). https://doi.org/10.1038/s41598-025-07261-6
6. Wanode D, Nandurkar D, Ambatkar M, Rarokar N, Khedekar P. A Review of Research from 2012 to 2024 on Pyrazole-based Anticancer Agents with SAR Study. Curr Top Med Chem. 2025; https://doi.org/10.2174/0115680266370083250530180225
7. Xu Z, Zhuang Y, Chen Q. Current scenario of pyrazole hybrids with in vivo therapeutic potential against cancers. Eur J Med Chem. 2023;257:115495. https://doi.org/10.1016/j.ejmech.2023.115495
8. Zala M, Vora JJ, Patel HB. Synthesis, Characterization, and Comparative Study of Some Heterocyclic Compounds Containing Isoniazid and Nicotinic Acid Hydrazide Moieties. Russ J Org Chem . 2020 Oct 24;56(10):1795–800. https://doi.org/10.1134/S1070428020100218
9. Patil S V., Suryavanshi MB, Nagargoje DR, Kokate S V. Synthesis and Antimicrobial Evaluation of Some New Pyrazole Derivatives Containing Thiazole Scaffolds. 2022;46. https://doi.org/10.3390/ecsoc-25-11661
10. Buckingham J. Dictionary of organic compounds. Vol. 12. Chapman and Hall; 1982.
11. Eneama WA, Salman HH, Mousa MN. Synthesis of a new Isoxazolidine and evaluation antitumor activity in vitro against MCF-7 breast cancer cell line. Onkol i Radioter. 2023;17(11):1–8.
12. Caminero Gomes Soares A, Marques Sousa GH, Calil RL, Goulart Trossini GH. Absorption matters: A closer look at popular oral bioavailability rules for drug approvals. Mol Inform. 2023;42(11):1–12. https://doi.org/10.1002/minf.202300115
13. Truong J, George A, Holien JK. Analysis of physicochemical properties of protein-protein interaction modulators suggests stronger alignment with the “rule of five.” RSC Med Chem. 2021;12(10):1731–49. https://doi.org/10.1039/D1MD00213A
14. Alsaad H, Kubba A, Tahtamouni LH, Hamzah AH. Synthesis, docking study, and structure activity relationship of novel anti-tumor 1, 2, 4 triazole derivatives incorporating 2-(2, 3-dimethyl aminobenzoic acid) moiety. Pharmacia. 2022;69(2):415–28. https://doi.org/10.3897/pharmacia.69.e83158
15. Shamsee ZR, Al-Saffar AZ, Al-Shanon AF, Al-Obaidi JR. Cytotoxic and cell cycle arrest induction of pentacyclic triterpenoides separated from Lantana camara leaves against MCF-7 cell line in vitro. Mol Biol Rep. 2019;46(1):381–90. https://doi.org/10.1007/s11033-018-4482-3
16. Synthesis and biological activity of potential antiviral compounds through 1,3-dipolar cycloadditions. Part 2: nitrones, nitrile oxides and imines, and other 1,3-dipoles Giuseppe Faita, Mariella Mella and Paolo Quadrelli.
17. Eneama WA, Salman HH, Mousa MN. Isoxazolidine Derivatives Exhibit Selective Antitumor Activity Against Breast Cancer Cells. Acad Open. 2023;9(2):1–18. https://doi.org/10.21070/acopen.9.2024.8148
18. Dhonnar SL, Sadgir NV, Adole VA, Jagdale BS. Molecular Structure, FT-IR Spectra, MEP and HOMO-LUMO Investigation of 2-(4-Fluorophenyl)-5-phenyl-1, 3,4-oxadiazole Using DFT Theory Calculations. Adv J Chem Sect A. 2021;4(3):220–30.
19. Abd AM, Salman HH, Mousa MN. Synthesis of some new Oxadiazoline Derivatives from 6-Methyl Nicotinate. European Journal of Modern Medicine and Practice. 2024;9(4):172-184. Available at: https://zenodo.org/records/13740445
20. Drozdowska K, Welearegay T, Österlund L, Smulko J. Combined chemoresistive and in situ FTIR spectroscopy study of nanoporous NiO films for light-activated nitrogen dioxide and acetone gas sensing. Sensors Actuators B Chem. 2022;353. https://doi.org/10.1016/j.snb.2021.131125
21. Salman HH, Ali MAM, Ali ET. Synthesis and screening of anticancer potentials of some new terephthaldehyde-derived nitrone compounds. Trop J Pharm Res. 2020;19(2):341–9. https://doi.org/10.4314/tjpr.v19i2.17
22. Ahmed AA, Turki AA, Hanoosh WS. Synthesis, Characterization of Some New Dimer Nitrone Deriv- atives from Dapsone, Their Use as Initiators for Polymerization. 2024;03(03):236–48. https://doi.org/10.51699/ijbea.v3i3.10
23. Salman HH, Mohammad-Ali MA, Al-Safe M. Antimicrobial evaluation of some new nitrone compounds derived from glyoxal. Int J Green Pharm. 2019;13(3):275–80.
24. Baren MH, Ibrahim SA, Al-Rooqi MM, Ahmed SA, El-Gamil MM, Hekal HA. A new class of anticancer activity with computational studies for a novel bioactive aminophosphonates based on pyrazole moiety. Sci Rep.

2023;13(1):1–20. https://doi.org/10.1038/s41598-023-40265-8
25. Culcasi M, Delehedde C, Esgulian M, Cassien M, Chocry M, Rockenbauer A. New Biocompatible β-Phosphorylated Linear Nitrones Targeting Mitochondria: Protective Effect in Apoptotic Cells. ChemBioChem. 2023;24(8). https://doi.org/10.1002/cbic.202200749
26. Shalaby MA, Fahim AM, Rizk SA. Microwave-assisted synthesis, antioxidant activity, docking simulation, and DFT analysis of different heterocyclic compounds. Sci Rep. 2023;13(1):1–21. https://doi.org/10.1038/s41598-023-31995-w
27. Zainuri DA, Hashim NNN, Affandi NS, Jamsari NJ, Razak IA. Anthracenyl chalcone: a promising anticancer agent—structural and molecular docking studies. Eur Phys J B. 2024;97(11):1–11. https://doi.org/10.1140/epjb/s10051-024-00822-0
28. Zhou H, Fu H, Shao X, Cai W. Identification of novel inhibitors for epidermal growth factor receptor tyrosine kinase using absolute binding free-energy simulations. Int J Biol Macromol. 2025;140989. https://doi.org/10.1016/j.ijbiomac.2025.140989
29. Quodbach J, Preis E, Karkossa F, Winck J, Finke JH, Steiner D. Novel Strategies for the Formulation of Poorly Water-Soluble Drug Substances by Different Physical Modification Strategies with a Focus on Peroral Applications. 2025;1–43. https://doi.org/10.3390/ph18081089
30. Zengin M, Tan OU, Arafa RK, Balkan A. Design and synthesis of new 2-oxoquinoxalinyl-1, 2, 4-triazoles as antitumor VEGFR-2 inhibitors. Bioorg Chem. 2022;121:105696. https://doi.org/10.1016/j.bioorg.2022.105696
31. Odah OA. Synthesis, Characterization, Anticancer Activity Study of Novel Curcumin Analogues Against A549 Lung Cancer Cell Line. Cent Asian J Med Nat Sci. 2024;5(4):610–26.